

Evaluation of CFAR and Texture Based Target Detection Statistics on SAR Imagery *

Lance M. Kaplan Romain Murenzi
Dept. of Engineering Dept. of Physics
Center for Theoretical Studies of Physical Systems
Clark Atlanta University
Atlanta, GA 30314
Email:{lmkaplan,murenzi}@pioneer.cau.edu

Abstract

In this work, we evaluated the effectiveness of synthetic aperture radar (SAR) target detection algorithms that consist of any number of combinations of three statistics which include two-parameter CFAR, variance, and extended fractal features. The performance of these algorithms were tested at various threshold settings over the public domain MSTAR database. This database contains one foot resolution X-band SAR imagery. Receiver-operating-characteristic (ROC) curves were generated for the seven resulting algorithms. The results indicate that the CFAR statistic is the least effective detection statistic.

1 Introduction

Automatic target detection/recognition (ATD/R) systems are required to detect and identify many different types of targets by processing over large amounts of image data. These systems should operate in near real-time where the ATR system can completely analyze an image before the next image can be formed by the sensor of choice. Many ATD/R systems are divided into three processing stages to lower the data throughput at the final recognition stage [5]. The three stages of a general ATD/R algorithm consists of a focus of attention (FOA) algorithm (or first level detection) to find hot spots in the image, a second level detection to remove false alarms due to clutter, such as trees and buildings, and a final recognition stage to identify and classify the targets that passed the initial two stages. The computational complexity of the FOA stage must be low since all pixels of the image must be screened at this stage.

In the past, researchers have exploited the fact that the intensity of a target pixel is on average higher than the intensity of the clutter background. Constant false alarm rate (CFAR) detectors threshold a normalized pixel intensity so that the false alarm rate remains

constant over the entire scene even if clutter intensity changes [4, 9]. Unfortunately, these CFAR detectors do not exploit the fact that targets have spatial extents which cover a number of pixels, and the distribution of intensities differ between target and clutter pixels.

Recently, researchers have considered the local distribution of intensities surrounding a pixel to develop statistics that respond to texture. For example, Subotic *et al.* uses differences in the phase information from targets and clutter [10] and Pham *et al.* combines a local variance feature and traditional grayscale features [8]. In [3], we introduced features derived from multiscale Hurst parameters which are able to detect large target sized objects while ignoring the objects too small to be a target.

In this paper, we test how detection algorithms, which fuse any number of combinations of a CFAR, variance, and extended fractal statistics, perform on real data. Section 2 describes our skeleton detection algorithm, and Section 3 reviews the three detection statistics. The experimental results presented in Section 4 are useful for a designer to determine which combination of detection statistics should be implemented in a real ATR/D system.

2 Generic Target Detection

In this paper, we want to compare the performance of each detection statistic solely on the basis of information each statistic provides. To this end, we tested the performance of a three stage generic detector. The first stage is the statistic calculation where the value for any of the detection statistics described in Section 3 are computed for each pixel in the image. The second stage generates a binary image by labeling pixels as targets if their statistic exceeds a threshold. The second stage may also include morphology so that if some detection clusters are too small, they are removed by a opening operation. Morphology mitigates false alarms by removing objects that are not target size. Finally, the last stage clusters the detections in the binary image into a number of centroids which represent the center of regions of interest (ROI) which are passed to later stages on the ATD/R system. If

*Prepared through collaborative participation in the Advanced Sensors Consortium sponsored by the U.S. Army Research Laboratory under Cooperative Agreement DAAL01-96-20-0001.

more than one detection statistic is used in the detector, our algorithm fuses the detection statistic after clustering, where the cluster centroid from one statistic is retained only if it resides near a cluster centroid extracted from the other statistics under investigation.

Note that morphological processing on the binary image actually includes spatial reasoning to the detector. To make our initial comparison fair, we decided to compare the statistics by implementing the generic detection algorithm without using any morphological operations. In future work, we plan to provide a systematic study of the optimal performance gain morphological processing can provide for each detection statistic.

3 Detection Statistics

The data requirements for the entire ATR algorithm require that the computational complexity of the FOA stage be as low as possible. Given an $N \times N$ image $I[m, n]$, the computational requirements to calculate the detection statistic at each pixel should not exceed $O(N^2)$ so that the complexity per a pixel is independent of image size. Efficient implementation of methods to compute the three detection statistics under investigation do, in fact, require only $O(N^2)$ operations. A description of each statistic follows below.

3.1 Two Parameter CFAR

The two parameter CFAR detection statistic has been used for many years as a detection statistic in an ATR system [5]. This CFAR statistic assumes the surrounding clutter grayscales follow a Gaussian distribution. Then, the pixel intensity $I[m, n]$ is normalized to keep false alarms constant over the entire image by $\hat{\sigma}[m, n]$, i.e.

$$C[m, n] = \frac{I[m, n] - \hat{\mu}[m, n]}{\hat{\sigma}[m, n]}. \quad (1)$$

The mean $\hat{\mu}[m, n]$ and standard deviation $\hat{\sigma}[m, n]$ for the clutter are estimated over a one pixel wide square annular window containing N_c elements surrounding the pixel under test. The annular window is large enough to surround the entire target.

3.2 Variance

The variance feature exploits the fact that the physical target of interest is composed of sharp edges which cause a few strong corner reflector returns inside target regions of the SAR image [8]. On the other hand, natural clutter consists of a number of reflecting surfaces which do not dominate the region. As a result, the variance of grayscales for pixels representing a target are usually larger than those representing clutter regions. Therefore, the variance statistic

$$V[m, n] = \hat{\sigma}_t^2[m, n] - \hat{\sigma}_c^2[m, n], \quad (2)$$

can indicate the pixel under test is a target when $V[m, n]$ is large. Note that similar to the CFAR case, the clutter variance $\hat{\sigma}_c^2[m, n]$ is computed over a one cell wide square annular window containing N_c elements which surrounds the pixel. The target variance

$\hat{\sigma}_t^2[m, n]$ is computed over a $W_t \times W_t$ solid square window surrounding the pixel $[m, n]$. W_t is chosen to correspond to the size of a typical target.

3.3 Extended Fractal Statistic

The extended fractal statistic is derived from multiscale Hurst parameters that generalize the Hurst parameter for fractional Brownian motion (fBm)[1]. The multiscale Hurst parameter measures the hyperbolic growth of the structure function at different scales. For an n -dimensional random process that satisfies the extended self-similarity condition, i.e.

$$\text{VAR}[B(\vec{t} + \vec{\tau}) - B(\vec{t})] = \sigma^2 f(\|\vec{\tau}\|), \quad \forall \vec{t}, \vec{\tau} \in \mathbf{R}^n, \quad (3)$$

the structure function is $f(\cdot)$. For fBm, the structure function is purely hyperbolic, i.e. $f(l) = l^{2H}$ where H is the Hurst parameter. The Hurst parameter is inversely proportional to the fractal dimension $D = n + 1 - H$ [6] so that roughness is inversely proportional to the Hurst value. In general, the fractal dimension of a process with stationary increments is determined by the scaling behavior of $f(l)$ as the incremental length l goes to zero.

A digital image can be modeled as a 2-D process satisfying (3) that is sampled every unit in both the x - and y - direction. When the digital image is subsampled by a factor of 2^s , the best guess to obtain the fractal dimension is made by measuring the scaling behavior at the two finest dyadic scales for the subsampled image, i.e.

$$\tilde{H}_s = \frac{1}{2} \log_2 \left(\frac{f(2^{s+1})}{f(2^s)} \right). \quad (4)$$

We refer to \tilde{H}_s as the *multiscale Hurst parameter* at scale s . As illustrated in [1], the generalized parameters provide clues about the apparent roughness of extended self-similar realizations at different scales. If the process happens to be fBm, then $\tilde{H}_s = H$ for all scales. In other words, fBm has constant roughness over all scales.

To estimate multiscale parameter locally at each pixel in an image $I[m, n]$, the structure function is estimated in the x - and y -directions by bootstrapping (3) so that

$$f_s^\theta[m, n] = \sum_{[m', n'] \in W_h[m, n]} |I[m' + 2^{s-1}, n'] - I[m' - 2^{s-1}, n']|^2, \quad \text{for } \theta = \{x, y\},$$

where $W_h[m, n]$ is a $W_h \times W_h$ window centered around pixel $[m, n]$. Then, the directed multiscale Hurst values are simply,

$$\tilde{H}_s^\theta[m, n] = \frac{1}{2} \log_2 \left(\frac{f_{s+1}^\theta[m, n]}{f_s^\theta[m, n]} \right), \quad \theta = \{x, y\}. \quad (5)$$

For simplicity, we develop an almost rotational invariant detection statistic by averaging the x - and y -directed Hurst value, $\tilde{H}_s[m, n] = (\tilde{H}_s^x[m, n] + \tilde{H}_s^y[m, n])/2$.

It has been known that local Hurst estimates can detect edges [2, 7]. The situation is identical for local multiscale Hurst estimates. In fact, the utility of the multiscale Hurst parameter as a detection statistic is due to its edge response for objects of different sizes as discussed in [3]. At fine scales, the local multiscale Hurst values provide high responses at the location of objects whose mean grayscales differ from the grayscales of the textured background in an image. As the scale increases to the point that the extended fractal features are computed using incremental lags greater than the object size, the local multiscale Hurst values go to zero. The size of the object can be determined by locating the scale where the Hurst estimates make the transition from a large value to a smaller value on par with the background values. Then, when the scale becomes large enough to require that the computation of the extended fractal features require incremental lags greater than the size of the sliding window, the Hurst response for an object becomes negative. The more negative the response, the larger the object. As a result, the negative of this extended Hurst value for $W_h = 65$ and $s = 5$ is used as the extended fractal statistic.

4 Experiments

We tested the seven resulting detection algorithms on the public domain MSTAR database which contains 2987 target chips and 100 pure clutter scenes covering approximately 10 square kilometers. The images were collected at X-band wavelengths with a resolution of one foot in both range and azimuth dimensions. In our experiments, we computed the probability of detection by computing the percentage of target chips which would pass the generic detection scheme at various operating points, i.e. threshold setting. Likewise, we counted the number of detections that the generic detection scheme provides over 100 clutter images at various operating points to compute the false alarm rate.

Figure 1 shows the plot of the receiver-operator-characteristic (ROC) curves for each of the seven detection methods. The ROC curve is the graph representing the detection probability versus false alarm rate at various operating points. Figure 1 indicates that for single statistic detection, the extended fractal feature provides the lowest false alarm rate at a given probability of detection. On the other hand, the CFAR statistic provides the highest false alarm rate. The figure also indicates that fusion of two statistics enhance detection performance with the exception that the extended fractal alone performed slightly better than the CFAR-variance fused detector. The best pair of statistics would be the variance and extended fractal features. Finally, the figure shows very little performance gain in using all three statistics instead of just using the variance and extended fractal features. This indicates that the CFAR statistic adds very little target information to the variance and extended fractal features.

To further illustrate the performance of each detector, we ran each detector on a clutter image where four targets were artificially embedded. Note that we

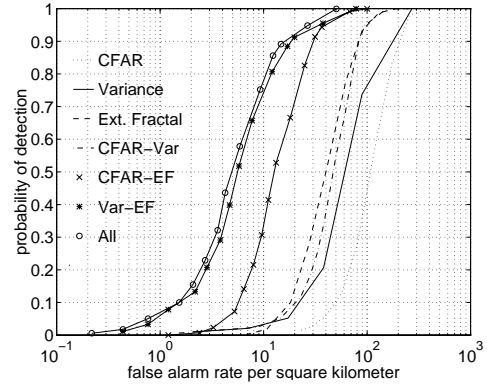


Figure 1: ROC curves.

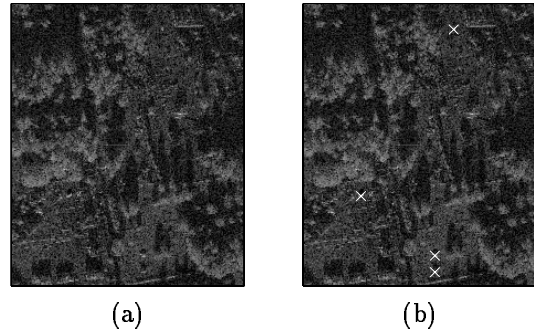


Figure 2: SAR Images: (a) Original and (B) with target markers.

set the thresholds of each statistics so that the probability of detection should be 0.8 based upon the results of Figure 1. The image contains a large number of cultural clutter elements which can confuse traditional CFAR detectors. Figure 2 shows the image with and without markers to indicate the target positions. Figure 3 shows images whose grayscales are proportional to the value of the detection statistics overlaid with labels indicating detections. The CFAR statistics provided the largest number of false alarms while completely missing one target. The fusion results are shown in Figure 4. This figure shows that the CFAR-variance still suffers from many false alarms (20 to be precise). The other fused statistics only generated 2 false alarms. Note that all detectors using the CFAR statistic missed one target.

5 Conclusions

The results of this paper indicate that extended fractal and variance detection statistics are superior than CFAR statistics for detection. The most likely reason for the lower CFAR performance is that the other statistics incorporate spatial relationship of target intensities. In fact, the performance of the ex-

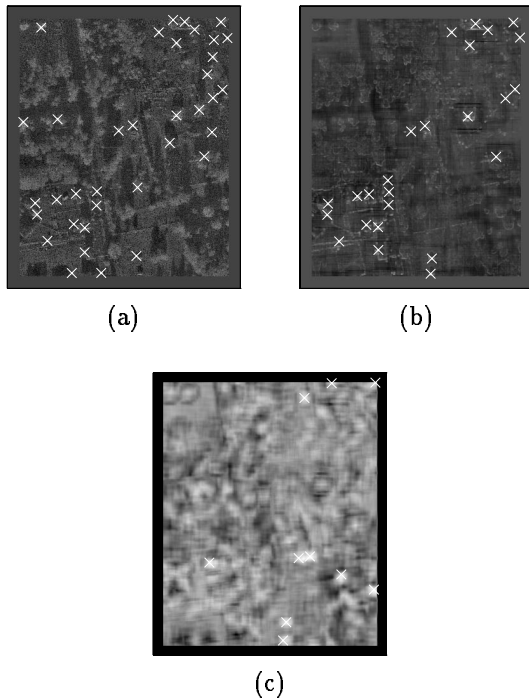


Figure 3: Detection statistics with detection markers: (a) CFAR, (b) variance, and (c) extended fractal.

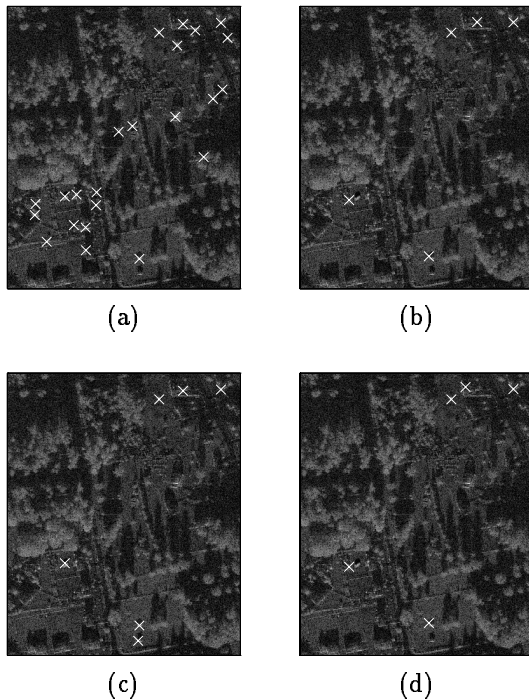


Figure 4: Detections using fused statistics: (a) CFAR-variance, (b) CFAR-extended fractal, (c) variance-extended fractal, and (d) all three.

tended fractal statistic may be better than the variance method because the extended fractal statistic can ignore single point-like scatterers due to cultural clutter, such as buildings. We plan to run these experiments on a more extensive database. We also plan to use optimization techniques to find the best morphological operations for each statistic to mitigate the false alarms. The morphological operations should add spatial information to the CFAR statistic. It would be interesting to see if CFAR performance can be enhanced through morphology to match the performance of the other two statistics. Finally, we plan to measure the ROC curves at varying levels of signal to clutter ratios (SCRs).

References

- [1] L. M. Kaplan and C.-C. J. Kuo, "Texture Roughness Analysis and Synthesis via Extended Self-Similar (ESS) Model," *IEEE Trans. on Pattern Analysis and Machine Intelligence*, Vol. 17, pp. 1043–1056, Nov. 1995.
- [2] L. M. Kaplan and C.-C. J. Kuo, "Texture Segmentation via Haar Fractal Feature Estimation," *Journal of Visual Communication and Image Representation*, Vol. 6, pp. 387–400, Dec. 1995.
- [3] L. M. Kaplan and R. Murenzi, "An Extended Fractal Based FOA Algorithm for SAR Imagery," in *6th Automatic Target Recognizer System and Technology Symposium*, Oct. 1997.
- [4] S. Kuttikkad and R. Chellappa, "Non-Gaussian CFAR Techniques for Target Detection in High Resolution SAR Images," in *IEEE ICIP 94*, pp. 910–914, Nov. 1994.
- [5] L. M. Novak, S. D. Halversen, G. J. Owirka, and M. Hiett, "Effects of Polarization and Resolution on SAR ATR," *IEEE Trans. on Aerospace and Electronic Systems*, Vol. 33, pp. 102–116, Jan. 1997.
- [6] H. O. Peitgen and D. Saupe, eds., *The Science of Fractal Images*, New York: Springer-Verlag, 1988.
- [7] A. P. Pentland, "Fractal-Based Description of Natural Scenes," *IEEE Trans. on Pattern Analysis and Machine Intelligence*, Vol. 6, pp. 661–674, Nov. 1984.
- [8] Q. Pham, T. M. Brosnan, and M. J. T. Smith, "A Reduced False Alarm Rate CFAR-based Prescanner for SAR ATR," in *Proceedings of the US Army Research Laboratory Sensors and Electron Devices Symposium*, Jan. 1997.
- [9] J. S. Salowe, "Very Fast SAR Detection," in *Proc. SPIE*, Vol. 2755, pp. 58–69, Apr. 1996.
- [10] N. S. Subotic, B. J. Thelen, J. D. Gorman, and M. F. Reiley, "Multiresolution Detection of Coherent Radar Targets," *IEEE Trans. on Image Processing*, Vol. 6, pp. 21–35, Jan. 1997.

DISCLAIMER

The views and conclusions contained in this document are those of the authors and should not be interpreted as presenting the official policies either expressed or implied of the Army Research Laboratory or the U. S. Government.